EigenFlux: A Stable Multi-Stream Radiative Transfer Method for Strongly Backward-Scattering Media

Daniel P. Johnson
Retired, Aerospace Research Fellow
Matthew S. Johnson
msj@chem.ku.dk

University of Copenhagen

Research Article

Keywords: Radiative Transfer, Asymmetrical Scattering, Atmospheric Physics, Light Propagation, Material Science, Remote Sensing

Posted Date: September 30th, 2025

DOI: https://doi.org/10.21203/rs.3.rs-3966645/v2

Additional Declarations: The authors declare no competing interests.

EigenFlux: A Stable Multi-Stream Radiative Transfer Method for Strongly Backward-Scattering Media

Daniel P. Johnson[1,*] **and Matthew S. Johnson**[2,*]

[1]Retired, Aerospace Research Fellow, Fridley, MN, USA

[2]Department of Chemistry, University of Copenhagen, Copenhagen Denmark

[*]drdpj@comcast.net, msj@chem.ku.dk

ABSTRACT

The radiative transfer (RT) of light and radiation through a medium such as an atmosphere, pigment, or water is of interest to many research communities, such as atmospheric physics and chemistry, metereology, climate research, astronomy, remote sensing, painting and coating material science, oceanography, hydrology, and graphics rendering. Despite its many uses, to the best of our knowledge there is not a non-commercial multi-stream algorithm capable of handling strongly backwards scattering systems with asymmetries in excess of -0.95. In this paper we present an derivation and implementation of the EigenFlux system which incorporates use of a Mesh Approximates multistream and eigenvalue decomposition with numerical stability achieved through the use of a natural reflectance condition. We conclude with numerical demonstrations of the range and precision of the method.

Introduction

The fundamental theory of light scattering in the atmosphere was developed by Lord Rayleigh in 1871[34]. Rayleigh scattering remains fundamental to the field of radiative transfer today. The earliest known formulations of the modern radiative transfer equation (RTE) were published by Eugen Von Lommel in 1887[25], and an integral version by Orest Chwolson in 1889[23]. However, neither publication spread to the general academic community[6].

In 1905, Schuster used hemispheric isotopy to develop and publish a two-stream RTE and its analytical solution[35] and has been traditionally credited with originating the RTE, although a similar two-stream approximation was presented by Eddington in 1916[11]. Papers by Schwarzschild in 1906 and 1914, and by Milne in 1921 on thermodynamic equilibrium within solar and stellar atmospheres led to the establishment of the RTE in its general form[24,36,37]. A full analytic theory of the RTE was developed and published by Chandresekhar in 1950[5].

In the meantime, Kubelka and Munk developed a simplified two-constant RTE and its solution in 1931[18,19] that is equivalent mathematically to Schuster's. Whereas Eddington and Shuster's two-stream RTE and subsequent modifications[21,29] have been considered only appropriate for mediums without strong asymmetry, Kubelka-Munk's method is accurate for determining the

reflectance of materials which are very strongly backscattering or forward-scattering. As a result, K-M and its modifications have become the standard for use by the painting and coating industries[17] where the most useful pigments tend to be those with extreme scattering properties.

A modern study which uses the K-M method is the Lawrence Berkeley National Laboratories study into pigments for roofing materials that show color in the visible spectrum, but are transparent in IR and UV so as to remain cool even under solar heating[1]. The study determined the scattering and absorbing properties of 85 candidate materials. Most materials were found to be strongly forward scattering[20].

Researchers in atmospheric physics/chemistry and oceanographers were interested in solutions to the full RTE in order to understand the effects of solar flux. The 1970's saw the development of a variety of RTE solvers starting from Chandresekhar's work[5], including the popular DISORT solver[39] available as public source code, both as a stand-alone distribution[22] and as part of the RadTranLib distribution[13].

Astronomers and metereologists were interested in the RTE as a way of understanding the albedo of the Earth and other planets[7]. Of interest here is the formulation and standardization of the Bi-Directional Radiation Field (BDRF)[27,43].

Application of the RTE to oceans began as early as 1922 when Raman[33] invoked scattering to explain the color of the sea. Scattering due to suspended particles and water turbulence play a major role in determining the color[38]. The resulting mathematics was given a firm footing by Preisendorfer's 6 Volume *Hydrologic Optics*[26,31,32]. The work of Akkaynak and Treibitz provides an interesting example of the use of the RTE in color-correction of underwater imaging[2].

The Hydrolight tool[15] is a commercial tool that can directly solve hydrological depth-varying absorbance and scattering problems, including systems with strong forward scattering. It is coded specifically for hydrological problems and does not address atmospheric radiative transfer or radiative transfer within pigmented materials.

A simplified form of the RTE was introduced by Blinn[3] as an approach to rendering realistic scenes in computer graphics in 1984. This was expanded into a generalized Light Transport Theory a few years later by Kajiya[16]. Although the initial impetus was primarily for models that are easy to compute and appear to be realistic, but are not necessarily accurate to the physics, advances in computer technology have allowed the increased use of physically-realistic models[30].

The complexity of rendering lighting and atmospheric effects in computer-generated imagery means that the leading rendering technology is based on ray-tracing and Monte-Carlo sampling. These methods provide an important alternative to the more traditional RTE solvers. An example is the MYSTIC code[12] which is included in the RadTranLib public source distribution[13] along with the more traditional DISORT solver[39].

The *Mesh Approximates* (MA) method presented here is closely related to the classic *Discrete Ordinates* (DO) method presented by Chandrasekhar[5] (we follow the presentation by Goody and Yung[14] and the paper by Stamnes, et al.[39]).

Both methods start with the integro-differential equation (3) with boundary conditions for the diffuse intensity with an explicit expression for the direct intensity.

DO first defines a finite-dimensional approximation of the integral terms to generate a linear ODE. That finite-approximation

uses a Legendre approximation of the phase matrix, and Gaussian quadrature for the integrals, which is mathematically equivalent to using Legendre polynomial expansions for the integrands.

To solve the resulting Ordinary Differential Equations (ODE), DO performs an eigenvalue decomposition to get a system of uncoupled ODEs, half of which are unstable. DO expresses the uncoupled ODEs and boundary conditions as an algebraic eigenvalue problem, which is then solved using specialized algorithms for that purpose.

MA first approximates the original equation using a piecewise-linear approximation of the phase matrix and the diffuse intensity, with exact evaluation of the resulting integrands over each piece-wise linear interval.

As in the previous method, the next step is to use an eigenvalue decomposition to solve the resulting Ordinary Differential Equations (ODE) to get a system of uncoupled ODEs, half of which are unstable. It stabilizes the uncoupled ODEs by initialing solving them using a natural reflectance assumption (equivalent to the assumption of an infinitely thick atmosphere). Piecewise-linear mesh approximations are again applied along the depth axis and to the boundary conditions in order to generate a well-conditioned linear system which can be solved with standard algorithms. The downward solution is then linearly combined with the reflected upward solution to generate the original two-boundary solution.

The DO method is limited by the fit using Legendre polynomials, which in particular converge slowly at the endpoints, making it difficult to use for strongly forward or backward scattering problems. The MA approach allows for the use of any subdivision of the ordinates, both for the multi-streams and along the depth axis. This allows for the use of meshes designed to resolve the underlying dynamics, for forward and backward scattering problems of up to ± 0.99 asymmetry for the existing implementations.

Like the DO, the MA is limited to application to plane-parallel homogeneous media. In both cases, the method is used to generate solutions to multiple layers with varying characteristics which can be combined into an overall heterogeneous solution.

Theoretical Development

We investigate *radiative transfer* though a homogeneous media, illuminated from its surface, that contains a uniform mix of pigment particles which may absorb or scatter light particles that are traveling through the media. We will limit this investigation to the plane-parallel situation, in which we only model the *depth* to which a light particle has penetrated, (increasing as the light particle descends deeper), the *relative velocity* (the cosine of the angle of travel relative to the vertical), and its *azimuth* (the angle of travel relative to the medium's "north").

The intensity function is interpreted here as the probability that a light particle is at depth y in the media, and has a relative velocity of v, where $v = cos(\theta)$. So ($v = 1$, $\theta = \pi/2$) is straight down, ($v = 0$, $\theta = 0$) is horizontal, and ($v = -1$, $\theta = -\pi/2$) is straight up.

The pigment particles may either absorb or scatter a light particle encountering them. This paper does not consider emission from the pigment, since that is a minor issue in determining color and transparency. The scatter distribution is determined by a rotationally symmetric phase function with asymmetry parameter g governing the degree of local backscatter versus forward

scatter.

Further information and background can be found in the references[14,17,29].

Key Variables and Functions

θ	Angle of travel of light particle, relative to vertical
ϕ	Azimuth of travel of light particle, relative to north
$v = \cos\theta$	Velocity relative to vertical
x	Depth
y	Depth scaled to extinction path length
z	Exponential depth $z = e^{-y/\hat{y}_{05}}$
$\tilde{I}(v,x,\phi)$	Intensity distribution
$I(v,y,\phi)$	Intensity distribution with respect to y
$s(v,\phi) = I(v,0,\phi)$	Intensity distribution at top boundary (source illumination)
$K(v,w)$	Normalized phase scattering distribution (parametrized by g)

Model Parameters

σ	Extinction path length for light to interact with pigment particles
ω	Single scatter albedo (=scattered/(scattered+absorbed))
g	phase function scattering asymmetry parameter
$\hat{y}_{05}$	two-stream estimate of the depth at which the transmission was reduced to 5% of the original source

Under stationary conditions, the intensity distribution (1) satisfies Schwartzchild's Equation[29]. Note that the emission term is not included as its contribution is not important for our intended application to pigment color.

$$\sigma\,\tilde{I}(v,x,\phi) + v\,\partial_x\tilde{I}(v,x,\phi) = \omega\,\sigma\int K(v,w)\tilde{I}(w,x,\phi)\,dw \tag{1}$$

After normalization with σ, this becomes

$$I(v,y,\phi) + v\,\partial_y I(v,y,\phi) = \omega\int K(v,w)I(w,y,\phi)\,dw \tag{2}$$

For pedagogical purposes we now choose to simplify the derivation by considering only azimuth-averaged input sources, allowing us to use an azimuth-independent formulation. See Subsection *Incorporating Azimuth-dependence* below for further details on the additional considerations for azimuth-dependent sources.

The *natural reflectance* of a material is the reflectance of a sample that is effectively opaque, e.g. adding additional depth does not change the reflectance significantly. In considering atmospheric radiation, this would be the assumption of an infinitely deep atmosphere (without the attendant pressure increase). In considering paints and coatings, this would be the assumption of a completely opaque film.

The left-hand side of equation (2) is a first-order linear differential equation in y, so we can write down the standard textbook solution with the initial boundary condition $s(v)$.

$$I(v,y) = s(v)\,e^{-y/v} + \omega(1/v)\,e^{-y/v}\int_{\eta=0}^{y}\int_{w=-1}^{1} e^{\eta/v}K(v,w)I(w,\eta)\,dw\,d\eta$$

However, for $v<0$, $e^{-y/v}$ is unbounded in y, and under the natural reflectance condition, the light exiting the surface, $I(v,0)$ for $v\le 0$ should be solely determined by the light entering the surface, $I(v,0)$ for $v\ge 0$.

By using a second boundary at depth M for the light moving up, we can get a two-sided equation in which we specify $I(v,0)$ for $v\ge 0$ for light moving from the surface to the bottom, and $I(v,M)$ for $v\le 0$ for light moving from the bottom to the surface.

For $v\ge 0$,

$$I(v,y) = s(v)\,e^{-y/v} + (\omega/v)\,e^{-y/v}\int_{\eta=0}^{y}\int_{w=-1}^{1} e^{\eta/v}K(v,w)I(w,\eta)\,dw\,d\eta$$

For $v<0$,

$$I(v,y) = s_M(v)\,e^{(M-y)/v} - (\omega/v)\,e^{-y/v}\int_{\eta=y}^{M}\int_{w=-1}^{1} e^{\eta/v}K(v,w)I(w,\eta)\,dw\,d\eta$$

Now apply the natural reflectance condition by letting $M\to\infty$ under the condition that $s_M(v)$ is bounded, which results in

For $v \geq 0$,

$$I(v,y) = s(v)\, e^{-y/v} + (\omega/v)\, e^{-y/v} \int_{\eta=0}^{y} \int_{w=-1}^{1} e^{\eta/v} K(v,w) I(w,\eta)\, dw\, d\eta$$

For $v < 0$,

$$I(v,y) = -(\omega/v)\, e^{-y/v} \int_{\eta=y}^{\infty} \int_{w=-1}^{1} e^{\eta/v} K(v,w) I(w,\eta)\, dw\, d\eta$$

As desired, the light exiting the surface, $I(v,0)$ for $v \leq 0$, is determined by the light entering the surface, $I(v,0)$ for $v \geq 0$.

Figure 1 shows the intensities for a strongly backscattering media.

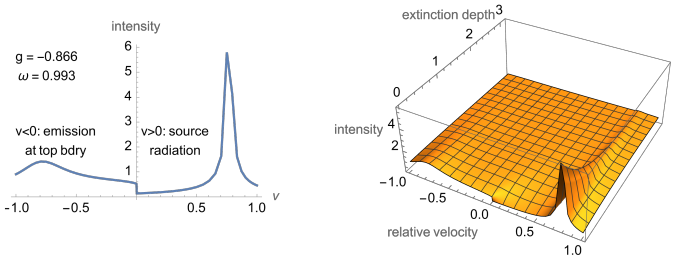

Figure 1. Intensities for strongly backscattering media: (left) source and emission radiation. (right) internal intensities.

Now we turn our attention back to the basic equation (2). This can be decomposed into two parts, the *direct* component which is the intensity of the source rays before they are scattered or absorbed (also known as *extinction*), and the *diffuse* component which is the intensity of the scattered light. Furthermore, we can immediately determine the form of the direct component,

We define the two components of the intensity as

$$R(v,y) = e^{-y/v} s(v) \qquad \text{Direct intensity distribution}$$
$$M(v,y) = I(v,y) - R(v,y) \qquad \text{Diffuse intensity distribution}$$

with the boundary condition $\forall v > 0, I(v,0) = s(v)$. Substituting these definitions into equation (2), we obtain the basic equation and side condition for the diffuse component.

$$M(v,y) + v\,\partial_y M(v,y) - \omega \int K(v,w)M(w,y)\,dw = \omega \int K(v,w)R(w,y)\,dw$$
$$\forall v > 0, M(v,0) = 0 \tag{3}$$

Figure 2 shows the internal direct intensity, which depends on the distribution of the source radiation and the extinction depth.

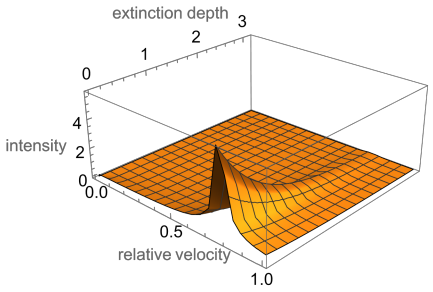

Figure 2. Internal direct intensity, depending on the distribution of the source radiation and the extinction depth.

Figure 3 shows the intensities for strongly forescattering and backscattering media.

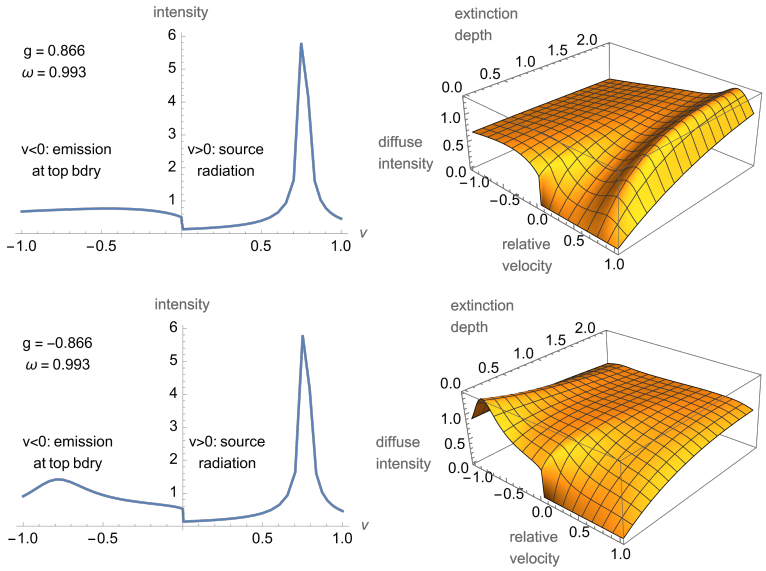

Figure 3. Internal diffuse intensities: (top) strongly forward scattering media, (bottom) strongly backscattering media.

We will be using a framework of basis functions and test functions to generate a *mesh approximation* for the various functions that consititute the full solution.

v_i	Approximation points for relative velocity
$\phi_i(v)$	Basis functions
$\psi_i(v)$	Test functions
$\tilde{f}(v) = \sum f_i \phi_i(v)$	Approximating form for 1D functions
$\tilde{h}(v,w) = \sum h_{ij} \phi_i(v) \phi_i(w)$	Approximating form for 2D functions

When seeking an approximate $\tilde{f}(v) \approx g(v)$, we expand $\tilde{f}$and integrate both against the test functions to get the linear equation which can be solved for the approximating coefficients.

$$\forall i, \sum_j f_i \int \psi_i(v) \phi_j(v)\, dv = \int \psi_i(v) g(v)\, dv$$

Any reasonable subdivision of points can be used for v_i. In this paper, v_i will be the concatenation of two sets of the Chebyshev points, one "arc" for $-1 \le v \le 0$ and another for $0 \le v \le 1$. The basis functions ϕ_i are triangular bump functions centered on the mesh points. We will be using two different choices for test functions in the course of this paper, either

1. $\psi_i = \phi_i$ where the test functions are the basis functions themselves, or

2. $\psi_i(v) = \delta[v = v_i]$ where the test functions are the Dirac delta functions, basically defining $\tilde{f}$ by sampling it at the mesh points.

Using (2) results in equations that are simpler, faster, and frequently better conditioned than (1), but using (1) preserves more of the symmetric properties of the original problem. So we use a mixture, (1) when additional symmetry is required, and (2) when expediency requires it.

To solve (3), we use an *eigenvalue expansion* of the linear system generated by the mesh approximation.

$K(v,w) = \sum_{jp} K_{jp} \phi_j(v) \phi_p(w)$	Phase function kernel
$s(v) = \sum_j s_j \phi_j(v)$	Intensity at surface
$M(v,y) = \sum_j M_j(y) \phi_j(v)$	Diffuse intensity distribution

From this we derive the finite dimensional linear ODE.

$$\sum_j A_{ij}\partial_y M_j(y) + \sum_j B_{ij}M_j(y) - \omega\sum_{jp} B_{ij}K_{jp}C_{pq}M_q(y) = \omega\sum_{jp} B_{ij}K_{jp}D_{pq}(y)s_q \tag{4}$$

where

$$A_{ij} = \int v\psi_j(v)\phi_j(v)dv$$

$$B_{ij} = \int \psi_j(v)\phi_j(v)dv$$

$$C_{ij} = \int \phi_j(v)\phi_j(v)dv$$

$$D_{ij}(y) = \int e^{-y/v}\phi_j(v)\phi_j(v)dv$$

More succinctly,

$$A\,\partial_y M(y) + (B - \omega BKC)M(y) = \omega BKD(y)s$$

The matrix A is near-singular at $v = 0$, but $(B - \omega BKC)$ is diagonally dominant and non-singular. So we can look at the eigenvalue decomposition of $(B - \omega BKB)^{-1}A$ for eigenvalues ν_k and eigenvectors Q_k. The resulting ODE becomes

$$\nu_k\partial_y\mu_k(y) + \mu_k(y) = \rho_k(y) \tag{5}$$

where

ν_k, Q_k	Eigenvalues and eigenvectors
$\mu_k(y)$	Eigenvector decoposition of $M_j(y)$
$\rho_k(y)$	Transformed boundary data

and

$$AQ_k = \nu_k(B - \omega BKC)Q_k$$

$$M_j(y) = \sum_k Q_k\mu_k(y)$$

$$\rho_k(y) = \omega Q^{-1}(B - \omega BKC)^{-1}BKD(y)s$$

Figure 4 shows the computed eigenvalues for varying parameter values.

Figure 5 shows the computed eigenvectors for a single set of the parameter values. Note in particular the all-positive eigenvectors for $\nu = \pm 1.8$. These are the limiting distributions of the intensity.

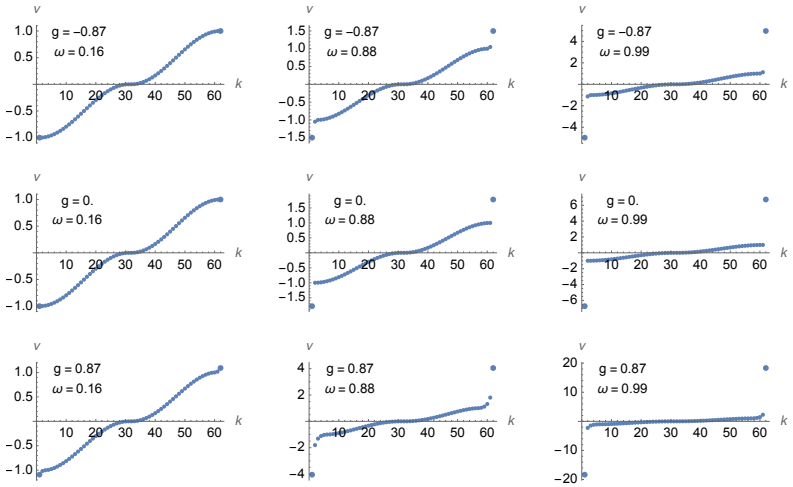

Figure 4. Eigenvalues for varying values of asymmetry g and scatter fraction ω.

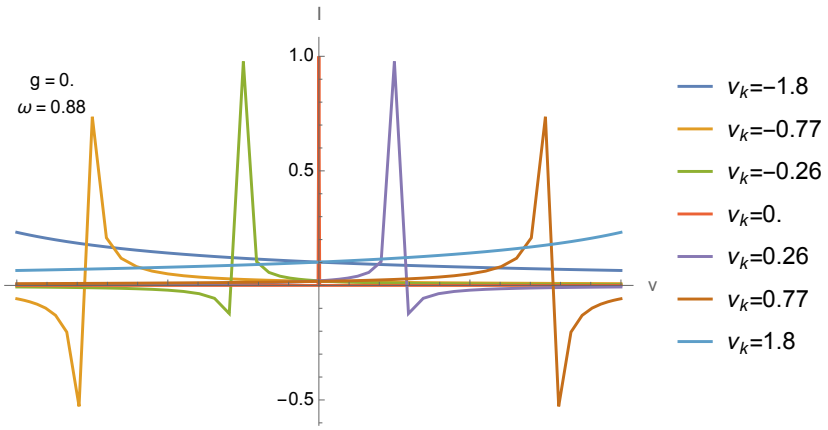

Figure 5. Sampling of eigenvectors for a single run.

We now have decomposed the problem into a set of one-dimensional first-order linear ODEs which have the general solution form

$$\mu_k(y) = \mu_k(0)e^{-y/\nu_k} + (1/\nu_k)\int_0^y e^{(\eta-y)/\nu_k}\rho_k(\eta)d\eta \tag{6}$$

However, there are two additional considerations–

One of the eigenvalues will be close to (or equal to) 0. In this case, we can go back to (5) and use the resulting condition $\mu_k(y) = \rho_k(y)$.

If the eigenvalue is negative, (6) would imply that we have an unstable mode. In this case, we can apply the natural reflectance assumption discussed previously to the new ODEs.

With these considerations, we have the following more specific solution.

$$\begin{aligned}
&\nu_k > 0 \implies \mu_k(y) = \mu_k(0)e^{-y/\nu_k} + (1/\nu_k)\int_0^y e^{(\eta-y)/\nu_k}\rho_k(\eta)d\eta \\
&\nu_k = 0 \implies \mu_k(y) = \rho_k(y) \\
&\nu_k < 0 \implies \mu_k(y) = -(1/\nu_k)\int_y^\infty e^{(\eta-y)/\nu_k}\rho_k(\eta)d\eta
\end{aligned} \tag{7}$$

Note in particular that this implies that for $k : \nu_k \leq 0$, $\mu_k(0)$ is determined by ρ_k (and hence by p_0). For positive ν_k, determination of $\mu_k(0)$ is slightly more complicated– they are determined by taking the side-condition $v > 0 \implies M[v,0) = 0$ (see (3)), expanding by $M_j(0) = \sum_k Q_k\mu_k(0)$ (see (5)) and solving for the unknown $\mu_k(0)$.

Finding a good approximation mesh for the depth y can be problematic because y has an unbounded range, so instead we use the exponential depth z where $z = e^{-y}$, $0 \leq z \leq 1$. With an abuse of notation, for a function of depth $f(y)$ we define $f(z) = f(-ln(z))$.

Similar to Step One, we apply the following mesh approximation to (7), (but now with $\bar{\psi}_i(z) = \delta[z = z_i]$, option (2) in the discussion on Mesh Approximation).

Depth Model Approximations

$$\begin{aligned}
\mu_k(y) &= \textstyle\sum_m \mu_{km}\phi_m(z) \text{ Transformed intensity} \\
\rho_k(z) &= \textstyle\sum_m \rho_{km}\phi_m(z) \text{ Transformed boundary conditions} \\
\rho_{kh} &= \omega Q^{-1}(B - \omega BKB)^{-1}BKD(z_h)p_0 \\
D_{ij}(z) &= \textstyle\int z^{1/v}\phi_j(v)\phi_j(v)dv
\end{aligned}$$

From this and (7) we get the following.

$$\begin{aligned}
&\nu_k > 0 \implies \mu_{km} = \mu_{0k}F_{kh} + (1/\nu_k)\rho_{km}G_{kmh} \\
&\nu_k = 0 \implies \mu_{km} = \rho_{kh} \\
&\nu_k < 0 \implies \mu_{km} = -(1/\nu_k)\rho_{km}G_{kmh}
\end{aligned}$$

where

$$F_{km} = z_m^{1/\nu_k}$$

and

$$\nu_k > 0 \implies G_{khm} = \int_0^1 \int_0^z z_h^{-1} (z_h/\zeta)^{1+1/\nu_k} d\zeta dz$$
$$\nu_k = 0 \implies G_{khm} = \chi[h = m]$$
$$\nu_k < 0 \implies G_{khm} = \int_0^1 \int_z^1 z_h^{-1} (z_h/\zeta)^{1+1/\nu_k} d\zeta dz$$

Taken together, these allow us to compute μ and M under the natural reflectance assumption.

Figure 6 shows the mesh points for relative velocity and exponential depth.

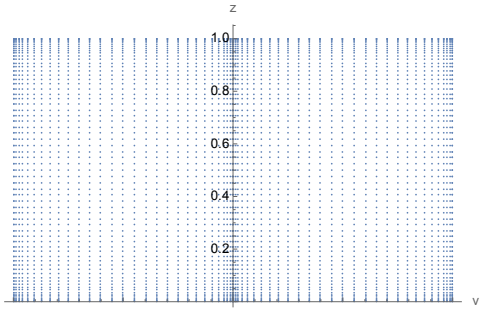

Figure 6. Mesh points for relative velocity and exponential depth.

The general solution for radiative transfer for a medium with finite depth and two boundaries, top and bottom can be expressed as the linear combination of a one-boundary solution for the top boundary and a one-boundary solution for the bottom boundary.

Let Φ be the fundamental solution for (3), so that $M = \Phi p_0$. With an abuse of notation, we replace the indices by the underlying mesh points e.g. $M_i(y) = M(v_i, y)$. We then note that the solution for a system with a bottom boundary is given by a depth-reversal of the solution for a system with a top boundary.

$$\tilde{M}^{top}(v_i, y) = \sum_{w_j \geq 0} \Phi(v_i, w_j, y)\, r_0(w_j)$$
$$\tilde{M}^{bot}(v_i, y) = \sum_{w_j \leq 0} {}^R\Phi(v_i, w_j, b-y)\, r_b(w_j) \tag{8}$$
$${}^R\Phi(v_i, w_j, b-y) = \Phi(-v_i, -w_j, b-y)$$

where

b	depth of bottom boundary
$\tilde{M}^{top}$	solution to top-boundary problem under natural reflectance assumption
$\tilde{M}^{bot}$	solution to bottom boundary problem under natural reflectance assumption
${}^{R}\Phi$	depth-reversed fundamental solution
$r_0(w_j)$	downwards illumination of top boundary ($w_j \geq 0$)
$r_b(w_j)$	upwards illumination of bottom boundary ($w_j \leq 0$)

Both the downwards and upwards system satisfy the base integro-differential equation (3). A linear combination of the two sets of solutions has the same degrees of freedom as the two-boundary problem, so a linear combination of the two will span the solution set.

To find that solution, first let's decompose the systems into downwards flows ($v \geq 0$) and upwards flows ($v \leq 0$).

$$\begin{bmatrix} I_y^{\uparrow} \\ I_y^{\downarrow} \end{bmatrix} = \begin{bmatrix} {}^{R}\Phi_{b-y}^{\downarrow} & \Phi_y^{\uparrow} \\ {}^{R}\Phi_{b-y}^{\uparrow} & \Phi_y^{\downarrow} \end{bmatrix} \begin{bmatrix} r_b^{\uparrow} \\ r_0^{\downarrow} \end{bmatrix}$$

where

$I_y^{\uparrow}$ Intensity of flow upwards at depth y

$I_y^{\downarrow}$ Intensity of flow downwards at depth y

From this we can determine the boundary input and output flows.

$$\begin{bmatrix} S_b^{\uparrow} \\ S_0^{\downarrow} \end{bmatrix} = \begin{bmatrix} {}^{R}\Phi_0^{\downarrow} & \Phi_b^{\uparrow} \\ {}^{R}\Phi_b^{\uparrow} & \Phi_0^{\downarrow} \end{bmatrix} \cdot \begin{bmatrix} r_b^{\uparrow} \\ r_0^{\downarrow} \end{bmatrix}$$

$$\begin{bmatrix} O_0^{\uparrow} \\ O_b^{\downarrow} \end{bmatrix} = \begin{bmatrix} {}^{R}\Phi_b^{\downarrow} & \Phi_0^{\uparrow} \\ {}^{R}\Phi_0^{\uparrow} & \Phi_b^{\downarrow} \end{bmatrix} \cdot \begin{bmatrix} r_b^{\uparrow} \\ r_0^{\downarrow} \end{bmatrix}$$

And so we have found the two-boundary system.

$$\begin{bmatrix} O_0^{\uparrow} \\ O_b^{\downarrow} \end{bmatrix} = \begin{bmatrix} {}^{R}\Phi_b^{\downarrow} & \Phi_0^{\uparrow} \\ {}^{R}\Phi_0^{\uparrow} & \Phi_b^{\downarrow} \end{bmatrix} \cdot \begin{bmatrix} {}^{R}\Phi_0^{\downarrow} & \Phi_b^{\uparrow} \\ {}^{R}\Phi_b^{\uparrow} & \Phi_0^{\downarrow} \end{bmatrix}^{-1} \cdot \begin{bmatrix} r_b^{\uparrow} \\ r_0^{\downarrow} \end{bmatrix}$$

where

$S_b^{\uparrow}$ Intensity of source input at bottom boundary at depth b

$S_0^{\downarrow}$ Intensity of source input at top boundary at depth 0

$O_0^{\uparrow}$ Intensity of output from top boundary

$O_b^{\downarrow}$ Intensity of output from bottom boundary boundary

Numerical Investigations

For the numerical experiments, the mesh approximation for the relative velocity v had 61 sample points distributed as two arcs of shifted Chebeyshev points, to give additional resolution around the three points $v = -1, 0, 1$. The mesh approximation for the scaled depths $0 \le z \le 1$ had 67 sample points distributed as shifted Chebeyshev points to provide additional resolution at $y = 0, \infty$. The actual scaling used was $z = e^{-y/\hat{y}_{05}}$ where $\hat{y}_{05}$ is the two-stream estimate of the depth at which the transmission was reduced to 5% of the original source. This provides better resolution by the numerical algorithm when the test case has strong backscattering or forward scattering.

The test cases used the Henyey-Greenstein phase function parametrized by g the asymmetry parameter, which in this case is equal to the average scatter angle relative to an incident angle.

The 957 test cases used all pairs of 33 values of the asymmetry parameter (= average scattering angle) g and 29 values of the scattering fraction ω (= probability of scatter given extinction, = 1 - probability of absorption given extinction).

var	definition	distribution	number	min	max
v_i	relative velocity	double chebyshev	61	-1	1
z_i	scaled exponential depth	chebyshev	67	0	1
g_i	asymmetry factor	chebyshev	33	-0.998867	0.998867
ω_i	single scatter albedo	modified chebyshev	29	0.0014660	0.9999995

Figure 7. Test case parameters

Figure 7 shows the parameters for the test cases. Figure 8 shows the mesh points for the asymmetry parameter and the single scatter albedo.

The Python implementation took 2.45 seconds per test case. The Mathematica implementation took 23.5 seconds per test case.

Asymptotic Diffusion Distribution

As shown in Figures 4 and 5 and discussed below, each material has a unique largest eigenvalue ν greater than 1 and a unique positive eigenvector. The rate of attenuation for each eigenvector is the reciprocal of the corresponding eigenvalue, so this

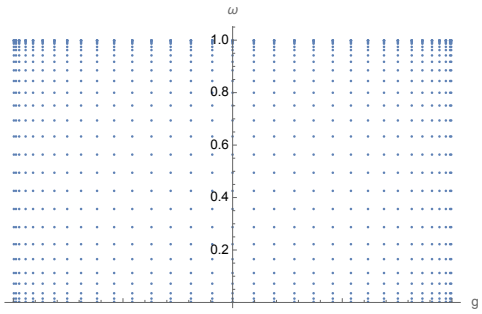

Figure 8. Mesh points for asymmetry parameter and the single scatter albedo

positive eigenvector has the slowest rate of attenuation among the diffuse components of the intensity. Since the largest eigenvalue is also greater than 1, it's rate of attenuation is also slower than the rate of attenuation of the direct component.

Hence the positive eigenvector represents the asymptotic limit of the distribution of the intensity as the optical depth increases, and the rate of convergence is given by the reciprocal of the eigenvalue. As shown in Figure 9, the maximum eigenvalue (and hence the slowest decay in diffusion) increases as absorption decreases ($\omega \to 1$) and as the forward scattering ratio increases ($g \to 1$).

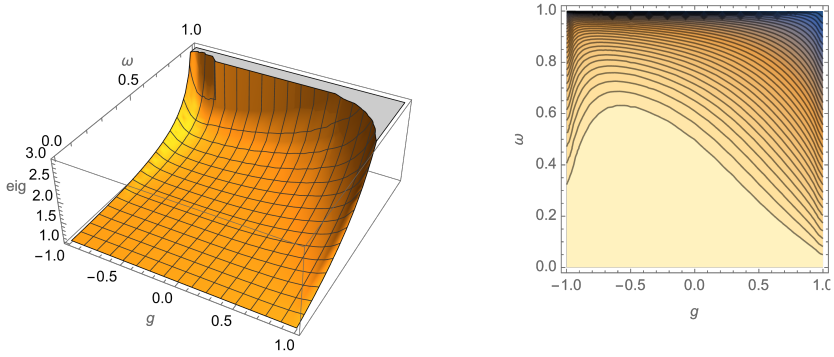

Figure 9. Maximum eigenvalues for varying asymmetry g and scatter fraction ω.

Of interest here is that the maximum eigenvalue is close to one on the majority of the region. Such materials have a very slow decay rate of diffusion relative to the direct component, so are in a strong sense effectively transparent. Given the direct component source in Figure 10, Figure 11 shows the convergence of an opaque material to the diffusion limit, while Figure 12 shows a semi-transparent material where the direct component remains larger than the limiting diffuse component.

A material is *semi-transparent* if it allows the direct component to come through the material. If we define the *semi-transparency depth* to be the maximum depth at which the direct component is at least 10% of the diffuse component, then any material which is thinner than its transparency depth will be semi-transparent. Figures 13 and 14 show the transparency depths and regions.

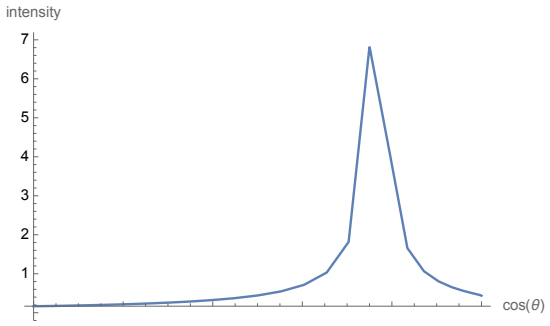

Figure 10. Direct source

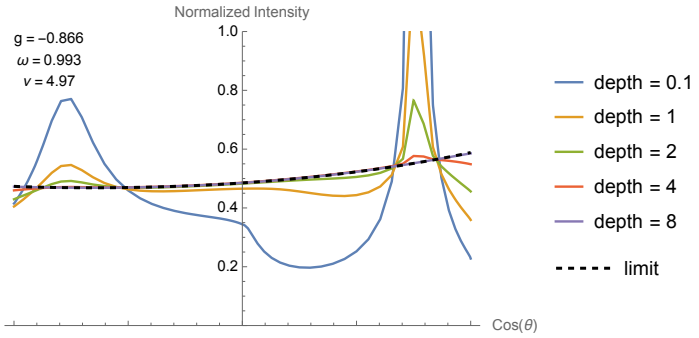

Figure 11. Convergence of normalized intensity distribution for $\nu \gg 1$.

Inherent and Apparent Optical Properties and the Difficulty of the Inverse Problem

The *Inherent Optical Properties*[26] (IOP) are the properties of a media that characterize its optical properties. For equation (1) they consist of the optical depth, the scatter fraction, and the scattering matrix. Since the numerical investigations here assume normalization by the optical depth and use the Henyey-Green one-parameter phase function, it is sufficient to use the scattering asymmetry g and the scattering fraction ω. This is also the common practice when using a two-stream approximation such as the Kubelka-Munk formulation.

The *Apparent Optical Properties*[26] (AOP) are the observed optical properties of a media. Following common practice, we look at the measured reflectance R and attenuation coefficient η.

The two-stream/Kubelka-Munk formulation provides simple analytic formulas for computing g and ω from R and η, and for the inverse. Unfortunately, numerical investigations show that the situation for the original problem is more complicated.

Figure 15 shows the reflectance and the attenuation coefficient at an optical depth of 0.75 for (a) $g = 0.85$ as ω varies from -1 to 1, (b) $\omega = -1$ as g varies from 0 to 1, and (c) $\omega = 1$ as g varies from 0 to 1, for the numerical simulation and for the two-stream analytic approximation.

This illustrates the following:

1. The two-stream approximation agrees with the full system on the four boundaries, $\omega = \pm 1$ and $g = 0, 1$,

2. Overall error of the two-stream approximation is ≈ 0.15 as shown in Figure 16.

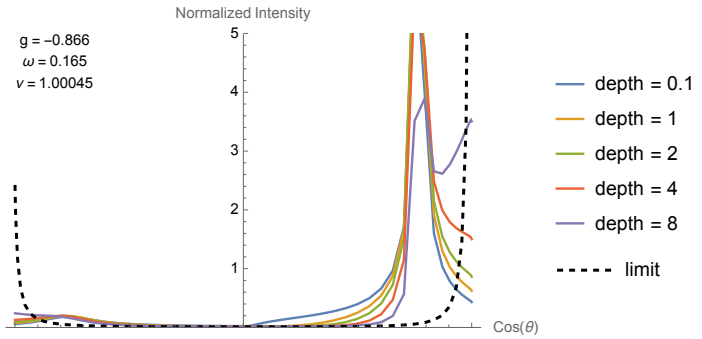

Figure 12. Convergence of normalized intensity distribution for $v \approx 1$.

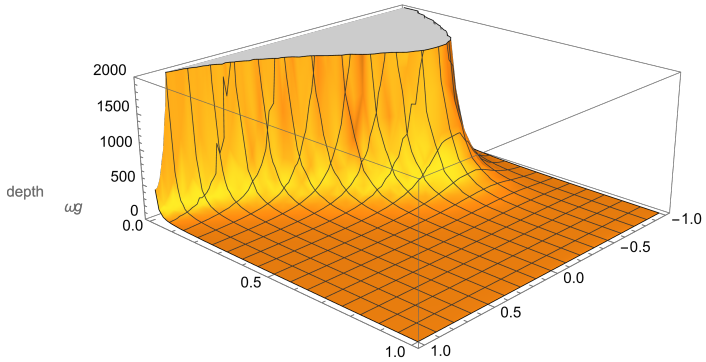

Figure 13. Semi-transparency depths for varying asymmetry g and scatter fraction ω.

3. The reflectance R and attenuation coefficient ξ_75 (at transmission loss 0.75) do not uniquely determine the asymmetry g and scatter fraction ω for $g < -0.7$.

If we look at the scatter diagrams at differing transmission loss depths in Figure 17, we see that the difficulty of invertibility increases as the loss increases, the data lets us determine g and ω at loss depths of less than 50%, or for $g > -0.5$, while inversion becomes problematic for loss depths greater than 75% and $g < -0.7$.

Methods

All numerical investigations were conducted on a MacBook Pro with 2.6 GHz 6-Core Intel Core i7, 16Gb of RAM, running Ventura V13.5.1. The final algorithm was coded in GNU Fortran 2008 as well as an implementation in Mathematica V13.1 using a Mathematica notebook, and Python V3.10.12 and numpy V1.25.1 using a Jupyter notebook V6.5.4. Six test cases were developed based on the DISORT distribution, and timing studies were run compared to DISORT using the same compiler.

The accuracy of the implementation was established by hand comparisons to published tables /citevanhulst1980 (Table 35).

In order to validate the fortran implementation of EigenFlux, the distribution for the standard radiative transfer package DISORT4 was downloaded from the *Light and Life Lab* website[22], along with its standard test suite. The Eigenflux software was then run on the DISORT test suite excluding the unimplimented features- thermal emissions and generalized BDRF

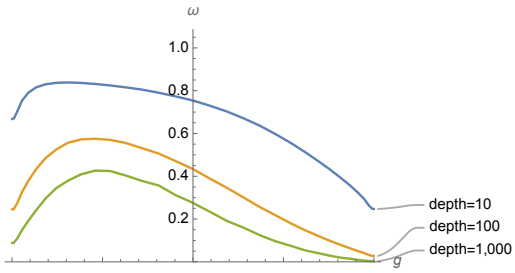

Figure 14. Regions for semi-transparency depths $10, 100, 1,000$.

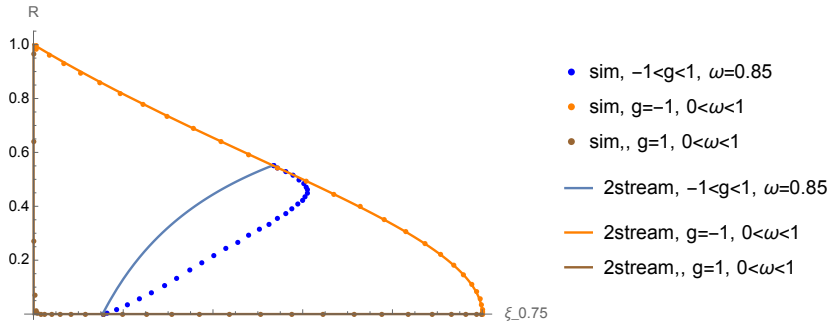

Figure 15. Reflectance and Attenuation Coefficient at 0.75 loss depth as computed by simulation and two-stream approximation.

functions, and compared to the reference DISORT results. See Figure 18.

Additional Topics

Hilbert Space Spectrum and Eigenvalues

In this section we show that much of the structure of the eigenvalues seen in figure 4 for a range of scattering fractions and asymmetry factors is reflected by the structure of the spectrum of the original equation (2) considered as a Hilbert space operator.

We exploit the spectral theory for Hilbert operators[9]. We rewrite the RHS of equation (2) as linear operators over the Hilbert space $L^2[-1,1]$ of measurable functions over the interval $[-1,1]$ with finite L^2 norm where

$$\begin{aligned} A[v]f(v) &= vf(v) \\ Kf(v) &= \int K(v,w)f(w)dw \\ \rho &= \omega BKD(y)p_0 \end{aligned} \tag{9}$$

and then (2) becomes

$$A[v]\partial_y M + (I - \omega K)M = \rho$$

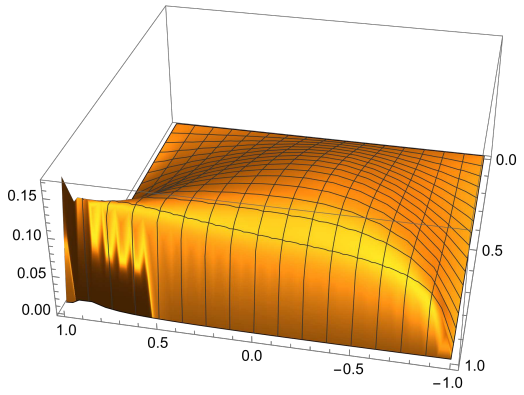

Figure 16. Absolute error in reflectance and attenuation coefficient for two-stream approximation, for $-1 < g < 1$ and $0 < \omega < 1$.

and now we can look at the spectrum of the operator

$$H = (I - \omega K)^{-1} A[v]$$

In general, the spectrum of a bounded operator B is comprised of three parts:

1. spec_d: A discrete spectrum of "true" eigenvalues (e.g. for $\nu \in \text{spec}(B)$, $\exists f \in L^2, Bf = \nu f$). The set will be finite or countable, with the only allowed limit point at $\nu = 0$.

2. essSpec: A continuous spectrum of approximate eigenvalues (e.g. for $\nu \in \text{essEpec}(N)$, there exists a sequence of unit functions $f_n \in L^2, ||Bf_n - \nu f_n|| \to 0$).

3. $\text{spec}_r = \text{spec}_d(B^*) \backslash (\text{spec}_d(B) \cup \text{essSpec}(B))$: A residual spectrum of eigenvalues of the adjoint operator which were not in spec_d or essSpec.

By its definition in (9), the operator K is an integral operator with doubly stochastic kernel, so is a compact operator. Since $H = A[v] + \omega KH$, this means that H is a compact perturbation of $A[v]$. $A[v]$ is also a Fredholm operator (provable through direct calculation of its kernel and co-kernels[9]). It then follows that $\text{essSpec}(A[v]) = \text{essSpec}(H)$, that the residual spectrum spec_r is empty, and that the remaining spectrum $\text{spec}_d(H) \backslash \text{essSpec}(H)$ consists of a finite number of isolated eigenvalues.

Furthermore, H is a positive operator on the positive half $[0,1]$ of the interval $[-1,1]$, so it has a maximum eigenvalue $\nu_{max} = ||H||$, and the corresponding eigenvector is positive and is the only positive eigenvector for that subspace.

Similar considerations for the negative half lead to the overall conclusion that H will have two isolated eigenvalues $\pm||H||$, each with a positive eigenvector, and those two eigenvectors are the only two positive members of the overall eigenspace.

From direct calculation on $A[v]$, we find that $A[v]$ (and therefore H) has a continuous distribution of spectrum values from -1 to 1, each value associated with a spectral function with a jump discontinuity at the spectrum value.

These conclusions are consistent with what we see in Figure 4 and Figure 5.

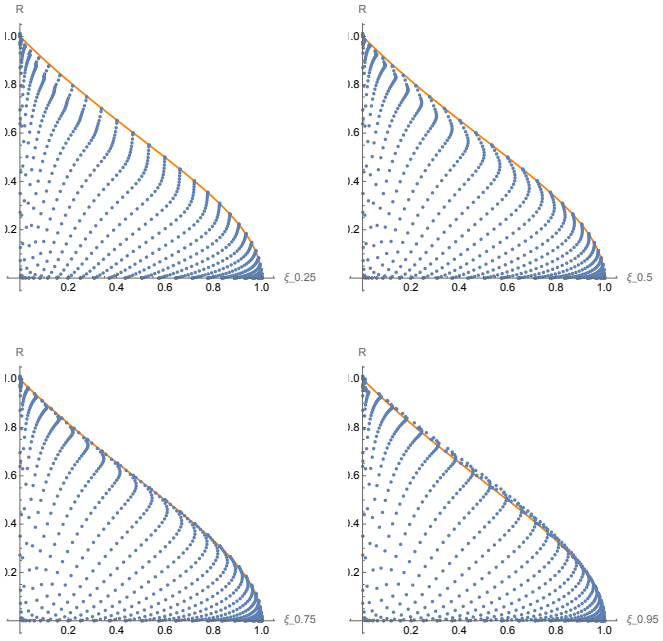

Figure 17. Scatter diagrams for reflectance R and attenuation coefficient ξ at loss depths of 25%, 50%, 75%, and 95%.

Test Case	EigenFlux (ms)	DISORT (ms)
1	340	404
2	200	310
3	104	33
4	9083	5188
5	4089	680
6	131	127

Figure 18. Test run results.

Incorporating Azimuth-dependence

Given a non-vertical collimated beam source, the intensity will be azimuth-dependent. While any azimuth dependence in the individual particles may be azimuth-dependent, it disappears when averaging over the random orientations of the particles. Nonetheless, even with a rotationally symmetric phase function, the scattering matrix will in general be azimuth-dependent.

Let the (averaged) phase function be given by $k(v)$. Then the scattering matrix will be given by

$$K(v_s, v_i; a_s - a_i) = k(v_s v_i + \cos(a_s - a_i)\sqrt{1 - v_s^2}\sqrt{1 - v_i^2}$$

where

(v_i, a_i) Polar cosine and azimuth angle of incident vector

(v_s, a_s) Polar cosine and azimuth angle of scattered vector

Under these conditions the main equation (2) becomes

$$\begin{aligned} I(v,a;y) + v\,\partial_y I(v,a;y) &= \omega \int K(v,w;a-b)P(w,b;y)\,dw \\ I(v,a;0) &= s(v,a) \end{aligned} \tag{10}$$

Note that $K(v,w;a)$ is cyclic in a, i.e. $K(v,w;a+2\pi) = K(v,w;a)$ and is the only term in the equation that is azimuth-dependent other than the boundary condition. As a result, the fundamental solution will be cyclically symmetric in azimuth

$$\Phi(v,a;w,b;y) = \Phi(v,a-b;w,0;y) = \Phi(v,a-b+2\pi;w,0;y)$$

We apply the mesh approximation process to the azimuth-dependent diffuse intensity equation (10) above) with the additional property that all functions/matrices (other than $p_0(v,a)$) that are dependent on azimuth are cyclically symmetric.

Model Approximations

$K(v,w;a-b) = \sum_{jpc} K_{jpc}\phi_j(v)\phi_p(w)\tilde{\phi}_c(a-b)$	Phase function kernel
$p_0(v;a) = \sum_{jc} p_{0jc}\phi_j(v)\tilde{\phi}_c(a)$	Intensity at surface
$M(v,y;a-b) = \sum_{jc} M_{jc}(y)\phi_j(v)\tilde{\phi}_c(a-b)$	Diffuse intensity distribution
$\tilde{\phi}_c(a-b) = \tilde{\phi}_c(a-b+2\pi)$	Azimuth test function

From this we derive the finite dimensional linear ODE.

$$\begin{aligned} &\sum_{jc} A_{ij}\tilde{B}_{fc}\partial_y M_{jc}(y) + \sum_{jc} B_{ij}\tilde{B}_{fc}M_{jc}(y) - \omega\sum_{jpc} B_{ij}\tilde{C}_{fdc}K_{jpd}B_{pq}M_{qc}(y) \\ &\qquad = \omega\sum_{jpc} B_{ij}\tilde{C}_{fdc}K_{jpd}D_{pq}(y)p_{0qc} \end{aligned} \tag{11}$$

where

$$A_{ij} = \int v\psi_j(v)\phi_j(v)dv$$

$$B_{ij} = \int \psi_j(v)\phi_j(v)dv$$

$$C_{ij} = \int \phi_j(v)\phi_j(v)dv$$

$$\tilde{B}_{fc} = \int \tilde{\psi}_f(a)\tilde{\phi}_c(a)da$$

$$\tilde{C}_{fdc} = \int \tilde{\psi}_f(a)\tilde{\phi}_d(a-b)\tilde{\phi}_c(b)da\,db$$

$$D_{ij}(y) = \int e^{-y/v}\phi_j(v)\phi_j(v)dv$$

More succinctly,

$$A\tilde{B}\partial_y M(y) + (B\tilde{B} - \omega B\tilde{C}KC)M(y) = \omega B\tilde{C}KD(y)p_0 \tag{12}$$

As before, the next step is to look at the eigenvalue decomposition of $\tilde{R} = (B\tilde{B} - \omega B\tilde{C}KB)^{-1}A\tilde{B}$. The matrix $\tilde{R}$ has some special properties:

1. $\tilde{R}$ is block circulant. I.e. $\tilde{R}_{fcij} = \tilde{R}_{(f-c)0ij}$
2. The individual blocks of $\tilde{R}$ are symmetric. I.e. $\tilde{R}^{fc}_{ij} = \tilde{R}^{fc}_{ji}$

Because of (1) and (2), the eigenvalues and eigenvectors of $\tilde{R}$ are real and can be determined from the number of blocks and the eigenvalue decomposition of a geometric sum of the individual blocks[8,40,41]. Let the blocks of $\tilde{R}$ be given by R_{i-j}. Let ρ be a primitive root of unity of order n, the number of blocks, so that $\rho^n = 1$ and such that $\{\rho^i\}$ generates a complete list of all roots of unity of order n. Let $H(\rho) = \sum_j \rho^j R_{n-j}$. Then the eigenvalues of $\tilde{R}$ are the $n*m$ eigenvalues of $H(\rho^k)$, and the eigenvectors are the outer product of $\{\rho^j_k\}$ and the eigenvectors of $H(\rho^k)$.

Data Availability

Materials described in the manuscript are available from the University of Copenhagen Electronic Research Data Archive at address: https://doi.org/10.17894/ucph.cfd8e267-97f3-496d-b434-e29984b931c8

References

1. Akbari, H., *et al.* "Cool colored materials for roofs" *Proceedings of American Council for an Energy Efficient Economy* Asilomar Conference Center in Pacific Grove, CA., Aug. 2004

2. Akkaynak, D. & Treibitz, T. "Sea-Thru: A Method for Removing Water From Underwater Images," *2019 IEEE/CVF Conference on Computer Vision and Pattern Recognition (CVPR)*, Long Beach, CA, USA, 2019, pp. 1682-1691, 2019

3. Blinn, J. F. "Light reflection functions for simulation of clouds and dusty surfaces" *Computer Graphics*, 16(3), 21-29 1982

4. Buras, R. & Mayer, B. "Efficient unbiased variance reduction techniques for Monte Carlo simulations of radiative transfer in cloudy atmospheres: The solution", *J. Quant. Spectrosc. Radiat. Transfer*, 112,434–447, 2011

5. Chandrasekhar, S. *Radiative Transfer*, Oxford Publications, Oxford, 1950 (reprinted Dover Publications, New York, NY, 1960.)

6. Chwolson, O. D. "Grundzüge einer mathematischen Theorie der inneren Diffusion des Lichtes". *Bull. Acad. Imp. Sci. St. Petersburg*, Nouvelle Série I (XXXIII), 221-256. 1889.

7. Coakley, J. A. "Reflectance and Albedo, Surface" *Encyclopedia of Atmospheric Sciences* Elsevier, 2003

8. Davis P.R. *Circulant Matrices*, John Wiley, New York. 1979.

9. Davis P.R. *Linear Operators and their Spectra*, Cambridge Studies in Advanced Mathematics 106, Cambridge University Press, Cambridge, UK. 2007.

10. d'Eon, E. *A Hitchhiker's Guide to Multiple Scattering* http://www.eugenedeon.com.hitchhikers

11. Eddington, A.S. "On the radiative quilibrium of the stars" *Monthly Not. of the Royal Astro. Soc.* 77, 16-35 1916

12. Emde, C., Buras, R., Mayer, B., & Blumthaler, M. "The impact of aerosols on polarized sky radiance: model development, validation, and applications", *Atmos. Chem. Phys.*, 10, 383–396, 2010.

13. Emde, C., *et al.* "The libRadtran software package for radiative transfer calculations (version 2.0.1)", *Geosci. Model Dev.*, 9, 1647–1672 2016

14. Goody, R. M. & Yung, Y. L. *Atmospheric Radiation, Theoretical Basis, 2nd Ed.*, Oxford University Press, New York 1989

15. HydroLight, *Radiative Transfer Software*, https://www.numericaloptics.com/hydrolight.html, 2020.

16. Kajiya, J. T. & Von Herzen, B. P. "Ray tracing volume densities" *Computer Graphics (Proceedings of SIGGRAPH '84*, Vol. 18, 165-74 1984

17. Koleske, J. V. (ed.), *Paint and Coating Testing Manual*, ASTM, Philadelphia, PA, 14th Edition, 1995.

18. Kubelka,P. & Munk, F. "Ein Beitrage zur Optik der Farbenstriche" *Zeitschrift Fur Technische Physik*, #12, p. 593 1931

19. Kubelka, P. "New Contributions to the Optics of Intensely Light Scattering Materialls– Part I" *Journal Optical Society of America*, #38, p448 1948

20. Levinson, R., Berdahl, P., & Akbari, H. "Solar spectral optical properties of pigments—Part I: model for deriving scattering and absorption coefficients from transmittance and reflectance measurements" *Solar Energy Materials and Solar Cells*, Volume 89, Issue 4, Pages 319-349

21. Liou, K. N. *An Introduction to Atmospheric Radiation, 2nd Ed.* Academic Press 2002

22. LLLab, "LLLab DISORT Website". Accessed July 21, 2023. http://www.rtatmocn.com/disort/

23. Lommel, E. "Die Photometrie der diffusen Zurückwerfung" *Sitzungsberichte der mathematische und physikalische Classe der Königlichen Bayerische Academie zu München*. 17, 95-132. 1887.

24. Milne, E. A. "Radiative Equilibrium in the Outer Layers of a Star: the Temperature Distribution and the Law of Darkening". *Monthly Notices Royal Astron. Soc*. 81(5), 361-375. 1921.

25. Mishchenko, M.I. "125 years of radiative transfer: Enduring triumphs and persisting misconceptions". *Radiation Processes in the Atmosphere and Ocean*. AIP Conf. Proc. 1531, 11-18. doi 10.1063/1.4804696. 2013.

26. Mobley, C.D. *Light and Water: Radiative Transfer in Natural Waters* Academic, San Diego. 1994

27. Nicodemus, F.E., Richmond, J.C., Hsia, J.J., Ginsberg, I.W. & Limperis, T. *Geometrical Considerations and Nomenclature for Reflectance*, National Bureau of Standards, October, 1977

28. NIST, *Digital Library of Mathematical Functions*, https://dlmf.nist.gov, Oct. 19, 2020.

29. Petty, G. W. *A First Course in Atmospheric Radiation*, Sundog Publishing, Madison, WI, 2nd edition, 2006.

30. M. Pharr, W. J. & Humphreys, G., *Physically Based Rendering, Fourth Edition: From Theory to Implementation*, MIT Press, 2023

31. Preisendorfer, R. W. "A survey of theoretical hydrologic optics", *Journal of Quantitative Spectroscopy and Radiative Transfer*, Vol. 8, Issue 1, Pages 325-338, 1968 https://doi.org/10.1016/S0022-4073(68)80116-5.

32. Preisendorfer, R. W. *Hydrologic Optics*, in 6 volumes: *Vol. 1: Introduction*, NTIS PB-259 793/8ST; *Vol. 2: Foundations*, NTIS PB-259 794/6ST; *Vol. 3: Solutions*, NTIS PB-259 795/3ST; *Vol. 4: Imbeddings*, NTIS PB-259 796/1ST; *Vol. 5: Properties*, NTIS PB-259 79719ST; *Vol. 6: Surfaces*, NTIS PB-268 704/4ST; Pacific Mar. Environ. Lab/NOAA, Seattle, WA. 1976

33. Raman, C.V. "On the molecular scattering of light in water and the colour of the sea" *Proc. R. Soc. Lond. A* 101:64–80 https://royalsocietypublishing.org/doi/10.1098/rspa.1922.0025 1922

34. Rayleigh, Lord., "On the light from the sky, its polarization and colour", *Phil, Mag.*,41:107-120. 274-279. 1871.

35. Schuster, A., "Radiation through a foggy atmosphere". *Astrophys. J*. XXI(I), 1-22. 1905.

36. Schwarzschild, K., "Ueber das Gleichgewicht der Sonnenatmosphäre". *Nachrichten von der Königlichen Gesellschaft der Wissenschaften zu Göttigen, Mathematische-Physikalische Klasse*, 195, 41-53. 1906.

37. Schwarzschild, K., "Über Diffusion and Absorption in der Sonnenatmosphäre". *Sitzungsberichte der Königlichen Preussischen Akademie der Wissenschaften*, 47, 1183-1202. 1914.

38. Shoulejkin, W. "On the Color of the Sea" *Phys. Rev. 22, 85* 1923

39. Stamnes, K., Tsay, S., Wiscombe, W. & Jayaweera, K., "Numerically stable algorithm for discrete-ordinate-method radiative transfer in multiple scattering and emitting layered media", *Applied Optics*, Vol. 27 page 2502, 1988

40. Tee, G.J. "A novel finite-difference approximation to the biharmonic operator", *The Computer Journal*, 6 (2), 177–192. MR29 #6646. 1963.

41. Tee, G. J. "Eigenvectors of Block Circulant and Alternating Circulant Matrices", *New Zealand Journal of Mathematics*, 36: 195–211. 2007.

42. Thomas, G. E., & Stamnes, K. *Radiative Transfer in the Atmosphere and Ocean*, Cambridge University Press, Cambridge, UK, 1999. 2005

43. Torrance, K.E. & Sparrow, F.M. "Theory for Off-Specular Reflection From Roughened Surfaces" *J. OSA*, Vol. 57, #9, 1105-1114, Sept. 1967

44. Van De Hulst, H. C., *Multiple Light Scattering, Tables, Formulas, and Applications, Vol 2*, Academic Press, New York 1980.